Article:

Absorption and unbounded superradiance
in a static regular black hole spacetime

Marco A. A. de Paula[1,2,*] Luiz C. S. Leite[3,†] Sam R. Dolan,[2,‡] and Luís C. B. Crispino[1,4,§]

[1]*Programa de Pós-Graduação em Física, Universidade Federal do Pará, 66075-110 Belém, Pará, Brazil*
[2]*Consortium for Fundamental Physics, School of Mathematics and Statistics, University of Sheffield,*
Hicks Building, Hounsfield Road, Sheffield S3 7RH, United Kingdom
[3]*Campus Altamira, Instituto Federal do Pará, 68377-630 Altamira, Pará, Brazil*
[4]*Departamento de Matemática da Universidade de Aveiro and Centre for Research and Development*
in Mathematics and Applications (CIDMA), Campus de Santiago, 3810-183 Aveiro, Portugal

Regular black holes (RBHs)—geometries free from curvature singularities—arise naturally in theories of nonlinear electrodynamics. Here we study the absorption and superradiant amplification of a monochromatic planar wave in a charged, massive scalar field impinging on the electrically charged Ayón-Beato-García (ABG) RBH. Comparisons are drawn with absorption and superradiance for the Reissner-Nordström (RN) black hole in linear electrodynamics. We find that, in a certain parameter regime, the ABG absorption cross section is negative, due to superradiance, and moreover it is unbounded from below as the momentum of the wave approaches zero; this phenomenon of "unbounded superradiance" is absent in the RN case. We show how the parameter space can be divided into regions, using the bounded/ unbounded and absorption/amplification boundaries. After introducing a high-frequency approximation based on particle trajectories, we calculate the absorption cross section numerically, via the partial-wave expansion, as a function of wave frequency, and we present a gallery of results. The cross section of the ABG RBH is found to be larger (smaller) than in the RN case when the field charge has the same (opposite) sign as the black hole charge. We show that it is possible to find "mimics": situations in which the cross sections of both black holes are very similar. We conclude with a discussion of unbounded superradiance and superradiant instabilities.

I. INTRODUCTION

General relativity (GR) is a geometric theory in which gravity is associated with the spacetime curvature generated by the presence of energy and momentum. For more than a century, the physical predictions of this theory have been scrutinized and tested experimentally in various ways [1–3]. In the last decade, for instance, two important verifications of GR predictions in the strong-field regime were reported: the Laser Interferometer Gravitational-Wave Observatory Collaboration performed the first direct detection of gravitational waves [4] from black hole (BH) coalescences, and

*marco.paula@icen.ufpa.br
†luiz.leite@ifpa.edu.br
‡s.dolan@sheffield.ac.uk
§crispino@ufpa.br

the Event Horizon Telescope (EHT) Consortium has obtained the first image of a supermassive BH shadow [5].

BHs are among the most fascinating predictions of GR. These objects are solutions of Einstein's field equations (EFEs) characterized by an event horizon (i.e., a nonreturn surface) and typically formed by gravitational collapse [6]. Observational evidence indicates that BHs populate galaxies [7]; for example, the Milky Way Galaxy harbors a supermassive BH (with $4.1 \pm 0.4 \times 10^6 M_\odot$ [8,9]) at its core, as well as myriad stellar-mass BHs.

In electrovacuum, the uniqueness theorems of GR [10] determine that stationary BH solutions are described by only three parameters: mass, charge, and angular momentum. Despite this apparent simplicity, the stationary BHs of GR are also paradoxical in nature: at their core is a "curvature singularity," where the classical field theory breaks down.

Key theorems that support the formation of curvature singularities in classical GR were established by Penrose [11] and Hawking and Ellis [12]. These theorems show that spacetimes can become geodesically incomplete in rather general (i.e., nonsymmetric) collapse scenarios, within the

classical field theory; and this, in turn, raises concerns about the global breakdown of causality in such spacetimes. As a remedy, the cosmic censorship hypothesis asserts that [11] all curvature singularities must be shrouded behind (apparent or event) horizons. Therefore, the spacetime outside this one-way membrane is not adversely affected by the presence of these hidden singularities.

It can be argued that the formation of singularities represents a flaw in *classical* field theory, and that the paradoxes associated with singularities will be fully resolved in a *quantum* theory of gravity. It is not necessary, however, to await a complete quantum theory before studying the properties of BH solutions that are free from singularities. Recently, there has been increasing interest in the properties of so-called regular black hole (RBH) solutions.

The first RBH model was proposed in 1968 by Bardeen [13]. In this model, as well as others [14–17], the source term (i.e., the stress-energy tensor) in the EFEs did not have a clear physical motivation or origin. In 1998, Ayón-Beato and García found that a RBH could arise in a physically well-motivated theory: nonlinear electrodynamics (NED) minimally coupled to GR [18].

NED models are, in essence, generalizations of Maxwell's linear theory to strong electromagnetic fields [19–22]. Two well-studied NED models are the Euler-Heisenberg model [23], which provides an effective description of quantum electrodynamics at the one-loop level, and the Born-Infeld model [19,20], introduced to remove the infinite self-energy of the electron. Among the features and applications of NED models [19–32], there have recently been proposed several electrically [33–38] and magnetically [39–45] charged RBH solutions, in minimally coupled GR, as well as in alternative theories of gravity [46–49]. For a review on NED and applications to BH physics, see Refs. [50,51].

In general, RBH geometries violate at least the strong energy condition in some region of the spacetime [52,53]. Furthermore, if the model satisfies the weak energy condition, as in the Bardeen case, then the topology is different from the Reissner-Nordström (RN) case [54]. Regarding NED-based electrically charged RBH solutions, the validity of the weak energy condition leads to de Sitter behavior in the RBH core [36], providing an effective cutoff on the self-energy density of the solution at the center.

Motivated in part by recent observational breakthroughs, there is growing interest in discerning how the key properties of RBHs will differ from those of irregular (i.e., singular) BHs, particularly in the observable region exterior to the horizon. A canonical example of the irregular class—and a key point of comparison for this study—is the RN spacetime: a spherically symmetric solution to the EFEs for *linear* (i.e., Maxwell) electromagnetism minimally coupled with GR, describing a BH of mass M and charge Q with two horizons, at $r_\pm = M \pm \sqrt{M^2 - Q^2}$, and a curvature singularity, at $r = 0$.

It is well known that the RN BH exhibits the phenomenon of superradiance when interacting with a scalar field of charge q. Field modes with a frequency $\omega > 0$ satisfying $\omega < q\phi_+$ are amplified, rather than absorbed, by the BH, where ϕ_+ is the electric potential at the outer horizon. In the superradiant regime, the BH loses charge and mass (i.e., it flows *out* of the BH into the field), and yet the area of the BH ($A = 4\pi r_+^2$) increases. In the thermodynamic interpretation, the horizon area is associated with the entropy of the BH, and superradiance is then a necessary consequence of the second law of thermodynamics. For studies about charged superradiance in static BHs, see, e.g., Refs. [55–62]. Superradiance can also occur with *neutral* fields if the BH is spinning. Superradiance has been studied in a range of BH scenarios over the past fifty years, leading to various interesting outcomes (see, e.g., Ref. [63] for a comprehensive review).

It is natural to ask whether superradiance persists for RBHs—and if so, whether it is enhanced or diminished. In the far-field region, $r \gg M$, where the electromagnetic field is weak, NED models are expected to reduce to linear electromagnetism, and thus, NED RBHs to be locally equivalent to RN BHs. Conversely, in the near-horizon region, where the electromagnetic field is strong, NED models are likely to differ substantially from their linear counterparts, and ϕ_+ may differ substantially from $\phi_+^{\text{RN}} = Q/r_+$. Consequently, we would expect the condition for superradiance to depend on the precise form of the NED model in question and, potentially, for certain models, to display enhanced versions of superradiance and new phenomenology. Some recent works addressed superradiance in the background of rotating regular spacetimes, considering massive scalar fields [64,65], but works considering charged scalar fields and superradiance in static RBH geometries are still lacking in the literature.

In this paper, we study the absorption of a charged massive test scalar field in the background of a RBH solution, namely, the first proposed exact charged RBH solution of Ayón-Beato and García (ABG) [18]. Here we are particularly interested in characterizing the effect of superradiance on the absorption cross section (ACS). Over the last fifty years, much effort has been made to compute absorption and scattering in different BH scenarios (cf., e.g., Refs. [66–74] and references therein). Although several works have been dedicated to chargeless test fields, few have dealt with the absorption of charged scalar fields [57,58]. Recently, the absorption of chargeless test fields has been investigated for RBHs [75–78], but the absorption of charged *massive* scalar waves is still to be properly quantified.

The remainder of this paper is organized as follows. In Sec. II, we review the main aspects of the ABG RBH spacetime proposed in Ref. [18], and in Sec. III we investigate the dynamics of a massive and charged scalar field on this spacetime. In Sec. III B, we present an

expression to compute the ACS via a sum over partial waves. In Sec. III C, we partition the parameter space, and in Sec. III D we describe a high-frequency approximation. Our numerical results concerning the absorption and superradiance properties of the ABG RBH solution are presented in Sec. IV, and we also compare them with those obtained in the RN case. We conclude with our final remarks in Sec. V. Throughout the paper we use the natural units, for which $G = c = \hbar = 1$, and metric signature -2.

II. FRAMEWORK

The action associated with NED minimally coupled to GR can be written as [18]

$$S = \frac{1}{4\pi} \int d^4x \left(\frac{1}{4}R - \mathcal{L}(F) \right) \sqrt{-g}, \qquad (1)$$

where R is the Ricci scalar, $\mathcal{L}(F)$ is a gauge-invariant electromagnetic Lagrangian density, and g is the determinant of the metric tensor $g_{\mu\nu}$. The electromagnetic invariant F and the standard electromagnetic field tensor are given by

$$F = \frac{1}{4}F_{\mu\nu}F^{\mu\nu} \quad \text{and} \quad F_{\mu\nu} = 2\nabla_{[\mu}A_{\nu]}, \qquad (2)$$

respectively, where A_ν is the electromagnetic four-potential.

It is possible to represent NED in a different framework by introducing an auxiliary antisymmetric tensor

$$P_{\mu\nu} \equiv \mathcal{L}_F F_{\mu\nu}, \qquad (3)$$

where $\mathcal{L}_F \equiv \partial \mathcal{L}/\partial F$; and also a structural function $\mathcal{H}(P)$ through a Legendre transformation [79], namely,

$$\mathcal{H}(P) \equiv 2F\mathcal{L}_F - \mathcal{L}(F). \qquad (4)$$

The invariant associated with $P_{\mu\nu}$ is defined as

$$P \equiv \frac{1}{4}P_{\mu\nu}P^{\mu\nu}. \qquad (5)$$

Among its applications [22,79], this framework is useful to obtain electrically charged NED-based RBH solutions [37].

With the help of Eqs. (2)–(5), one can show that

$$P = (\mathcal{L}_F)^2 F, \quad \mathcal{H}_P\mathcal{L}_F = 1, \quad \text{and} \quad F_{\mu\nu} = \mathcal{H}_P P_{\mu\nu}, \qquad (6)$$

where $\mathcal{H}_P \equiv \partial \mathcal{H}/\partial P$. By varying the action (1) with respect to the inverse metric tensor $g^{\mu\nu}$ and using Eqs. (6), it is possible to obtain

$$G^\mu_\nu = -T^\mu_\nu = 2[\mathcal{H}_P P_{\nu\alpha}P^{\mu\alpha} - \delta^\mu_\nu(2P\mathcal{H}_P - \mathcal{H})], \qquad (7)$$

which are Einstein-NED field equations, and where G^μ_ν is the Einstein tensor and T^μ_ν is the energy-momentum tensor.

The variation of the action (1) with respect to A_μ leads to $\nabla_\mu P^{\mu\nu} = 0$ (in the absence of electromagnetic sources).

For the solution proposed in Ref. [18], from now on simply referred to as the ABG solution, the structural function (the NED source) is

$$\mathcal{H}(P) = P\frac{\left(1 - 3\sqrt{-2Q^2P}\right)}{\left(1 + \sqrt{-2Q^2P}\right)^3} - \frac{3M}{|Q|Q^2}\left(\frac{\sqrt{-2Q^2P}}{1 + \sqrt{-2Q^2P}}\right)^{\frac{5}{2}}, \qquad (8)$$

with Q and M being the electric charge and mass of the central object, respectively. Considering a spherically symmetric and static line element as an ansatz for the spacetime, together with Eqs. (7) and (8), one can obtain the ABG line element in spherical coordinates ($x^\mu = \{t, r, \theta, \varphi\}$),

$$ds^2 = f(r)dt^2 - \frac{1}{f(r)}dr^2 - r^2(d\theta^2 + \sin^2\theta d\varphi^2), \qquad (9)$$

where

$$f(r) = f^{\text{ABG}}(r) \equiv 1 - \frac{2Mr^2}{(r^2 + Q^2)^{3/2}} + \frac{Q^2r^2}{(r^2 + Q^2)^2} \qquad (10)$$

is the metric function of the ABG spacetime.

In the asymptotic limit $r \to \infty$, the metric function (10) has the following behavior:

$$f^{\text{ABG}}(r) = f^{\text{RN}}(r) + \mathcal{O}(r^{-3}), \qquad (11)$$

where $f^{\text{RN}}(r)$ is the metric function of the RN spacetime [80],

$$f^{\text{RN}}(r) \equiv 1 - \frac{2M}{r} + \frac{Q^2}{r^2}. \qquad (12)$$

As argued earlier, this is expected because, in the far-field region, the electromagnetic field is weak and thus in the linear (i.e., Maxwell) regime. On the other hand, expanding the ABG metric function in powers of Q yields

$$f^{\text{ABG}}(r) = f^{\text{RN}}(r) + \frac{3MQ^2}{r^3} + \mathcal{O}(Q^4). \qquad (13)$$

When the condition $|Q| \leq Q_{\text{ext}} \approx 0.6341M$ is fulfilled [18], the line element (9) describes an ABG RBH. For $|Q| < Q_{\text{ext}}$, the ABG RBH possesses an inner (Cauchy) horizon at r_- and an outer (event) horizon at r_+, given by the real positive roots of $f^{\text{ABG}}(r) = 0$. For $|Q| = Q_{\text{ext}}$, we have the so-called "extreme" ABG RBH, with $r_+ = r_-$. For $|Q| > Q_{\text{ext}}$, we have horizonless solutions. The ABG causal structure is similar to the RN one (for which $Q^{\text{RN}}_{\text{ext}} = M$).

Throughout this work, we shall restrict our analysis to BH solutions ($|Q| \leq Q_{\text{ext}}$) and exhibit our results in terms of the normalized electric charge

$$\alpha \equiv \frac{Q}{Q_{\text{ext}}}, \tag{14}$$

which satisfies $0 \leq |\alpha| \leq 1$ for BH geometries.

From $F_{01} = E(r) = \mathcal{H}_P Q / r^2$, one can show that the radial electrostatic field $E(r)$ of the ABG solution is given by

$$E^{\text{ABG}}(r) = Qr^4 \left(\frac{r^2 - 5Q^2}{(r^2 + Q^2)^4} + \frac{15M}{2(r^2 + Q^2)^{7/2}} \right), \tag{15}$$

which is finite at the origin and asymptotically behaves as the electrostatic field in the RN case, given by

$$E^{\text{RN}}(r) = \frac{Q}{r^2}. \tag{16}$$

A detailed analysis of the metric function, electric field, and geodesics of massless particles of ABG and RN BHs is presented in Refs. [78,81].

The covariant components of the electromagnetic four-potential are given by

$$A_\mu = (\phi(r), 0, 0, 0), \tag{17}$$

where ϕ is the electrostatic potential, which can be obtained using $\phi(r) = -\int_\infty^r \mathbf{E} \cdot d\mathbf{l}$ and Eq. (15), to obtain[1]

$$\phi^{\text{ABG}}(r) = \frac{r^5}{2Q} \left(\frac{3M}{r^5} + \frac{2Q^2}{(Q^2 + r^2)^3} - \frac{3M}{(Q^2 + r^2)^{5/2}} \right). \tag{18}$$

In Fig. 1, we plot the ABG electrostatic potential $\phi^{\text{ABG}}(r)$ alongside the electrostatic potential of the RN BH,

$$\phi^{\text{RN}}(r) = \frac{Q}{r}. \tag{19}$$

Notably, $\phi^{\text{ABG}}(r)$ is finite at $r = 0$, whereas $\phi^{\text{RN}}(r)$ diverges as $r \to 0$. In the far field ($r \to \infty$), $\phi^{\text{ABG}} \to \phi^{\text{RN}}$. At the (outer) horizon, $\phi(r_+)^{\text{ABG}} > \phi(r_+)^{\text{RN}}$, and thus an enhanced superradiant regime may be anticipated.

_____

[1]We choose the infinity as the reference point at which the electrostatic potential is zero. If one adopts such reference point of the electrostatic potential at $r = 0$, it follows an expression for $\phi^{\text{ABG}}(r)$ that does not behave asymptotically as the RN electrostatic potential [82].
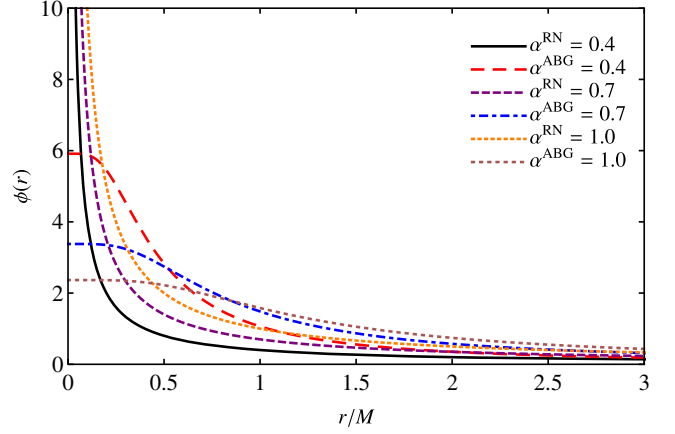

FIG. 1. Comparison between the electrostatic potentials of ABG and RN BHs, considering different values of α.

III. ANALYSIS

A. Scalar fields and superradiance

We are interested in investigating a scalar field Φ with mass μ and charge q, propagating in a static (electric) RBH spacetime. Therefore, we shall consider the Klein-Gordon equation

$$(\nabla_\nu + iqA_\nu)(\nabla^\nu + iqA^\nu)\Phi + \mu^2\Phi = 0. \tag{20}$$

Exploiting the separability of Eq. (20), we can write a particular mode of Φ as

$$\Phi \equiv \frac{\Psi_{\omega l}(r)}{r} P_l(\cos\theta) e^{-i\omega t}, \tag{21}$$

where $\Psi_{\omega l}(r)$ are radial functions and $P_l(\cos\theta)$ are the Legendre polynomials. The indexes ω and l denote the frequency and the angular momentum of the scalar wave, respectively. Inserting Eq. (21) into Eq. (20) leads to the radial equation

$$\frac{d^2}{dr_\star^2} \Psi_{\omega l} = V(r)\Psi_{\omega l}, \tag{22}$$

where $r_\star$ is the "tortoise coordinate" defined by $dr_\star = dr/f(r)$, and the potential function $V(r)$ reads

$$V(r) \equiv f(r)\left[\mu^2 + \frac{1}{r}\frac{df(r)}{dr} + \frac{l(l+1)}{r^2} \right] - (\omega - qA_0(r))^2. \tag{23}$$

From the form of Eq. (22), it is clear that Φ is propagative (i.e., oscillatory) in regions where $V(r) < 0$ and evanescent (i.e., exponential) in regions where $V(r) > 0$.

As the angular momentum l increases, the height of the potential barrier increases commensurately (as in the massless case [78]). Figure 2 shows $V(r)$ as a function of the parameter qM for the particular case $l = 0$, $\omega = \mu$,
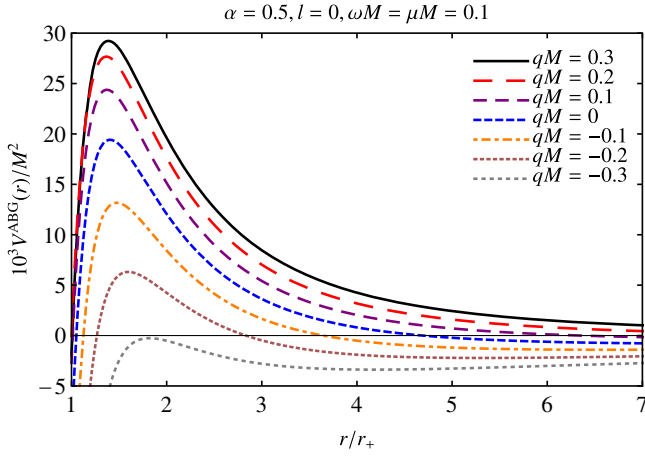
FIG. 2. The function $V(r)$ of charged massive scalar waves in the background of the ABG RBH, as a function of r/r_+, considering different values of qM. In this figure, we have chosen $l = 0$, $\omega M = \mu M = 0.1$, and $\alpha = 0.5$.

and $\alpha = 0.5$ [defined in Eq. (14)]. The height of the local maximum value of $V(r)$ increases with qM. As we increase α, the peak of $V(r)$ increases (decreases) for $qM > 0$ ($qM < 0$). This is anticipated from the Lorentz force: particles with the same charge sign of the BH are repelled, and consequently less absorbed, than particles with the opposite charge, which are attracted. Note also that, for some values of qM, μM, and α, the peak of the radial function $V(r)$ becomes negative (cf. curve $qM = -0.3$ in Fig. 2) [83].

In the (planar-wave) scattering problem, the wave satisfies the ingoing boundary conditions

$$\Psi_{\omega l} \sim \begin{cases} T_{\omega l} e^{-i\zeta r_\star}, & r_\star \to -\infty, \\ I_{\omega l} e^{-i\kappa r_\star} + R_{\omega l} e^{i\kappa r_\star}, & r_\star \to +\infty, \end{cases} \quad (24)$$

where $\zeta \equiv \omega - q\phi_+$ [with $\phi_+ \equiv \phi(r_+)$], and $\kappa \equiv \sqrt{\omega^2 - \mu^2}$. The quantities $T_{\omega l}$, $I_{\omega l}$, and $R_{\omega l}$ are complex coefficients.

Justification for the ingoing boundary condition in (24) runs as follows. In the near-horizon region, the general solution for the field Φ is a superposition of two terms, with behaviors $e^{-i(\omega t \pm \zeta r_\star)}$. We seek fields Φ and A_μ which are regular on the *future* horizon in a suitable gauge. Noting that, for A_μ in Eq. (17), the Lorentz invariant $A_\mu A^\mu$ is divergent, we can make a "gauge transformation," $A_\mu \to A'_\mu = A_\mu + q^{-1}\nabla_\mu \chi$ and $\Phi \to \Phi' = e^{i\chi}\Phi$, such that $A'_\mu = 0$ on the horizon. This corresponds to the choice $\chi = q\phi_+ t$. Hence, the general solution for Φ' is a superposition of two terms with behaviors $e^{-i\zeta(t \pm r_*)}$. The term with upper sign choice $(+)$ is regular (irregular) on the future (past) horizon, and the term with the lower sign $(-)$ is regular (irregular) on the past (future) horizon. The boundary condition in Eq. (24) then follows from the requirement that Φ' is regular on the future horizon.

For a propagating wave at infinity (unbounded modes), the condition $\kappa > 0$ holds, i.e., $\omega^2 > \mu^2$. The transmission and reflection coefficients are defined, respectively, as

$$|\mathcal{T}_{\omega l}|^2 \equiv \frac{|T_{\omega l}|^2}{|I_{\omega l}|^2} \quad \text{and} \quad |\mathcal{R}_{\omega l}|^2 \equiv \frac{|R_{\omega l}|^2}{|I_{\omega l}|^2}. \quad (25)$$

From the conservation of the flux, or using the Wronskian of Eq. (22), one can derive

$$|\mathcal{R}_{\omega l}|^2 + \frac{\zeta}{\kappa}|\mathcal{T}_{\omega l}|^2 = 1. \quad (26)$$

The "amplification factor" [63] is

$$Z_{\omega l} \equiv |\mathcal{R}_{\omega l}|^2 - 1 = -\frac{\zeta}{\kappa}|\mathcal{T}_{\omega l}|^2. \quad (27)$$

This measures the fractional gain (or loss) of energy in a scattered wave, with positive values of $Z_{\omega l}$ corresponding to superradiant amplification. Clearly, the sign of $Z_{\omega l}$ is determined by the sign of ζ. Hence the "critical frequency" for superradiant scattering is

$$\omega_c = q\phi_+. \quad (28)$$

For frequencies $\omega > \omega_c$, the wave is absorbed; conversely, for frequencies $0 < \omega < \omega_c$, the wave is amplified.

In Fig. 3, we show ϕ_+, the electric potential at the horizon, for ABG and RN BHs. We note that (for $\alpha > 0$) ϕ_+ is always positive and increases monotonically with α. As a consequence, superradiance occurs whenever $q\phi_+ > 0$. We also observe that ϕ_+^{ABG} is always greater than ϕ_+^{RN}. Therefore, for the same values of qM and α, the critical frequency of the ABG RBH is always larger than that of the RN BH. This implies a greater capacity for superradiant scattering in the ABG case.
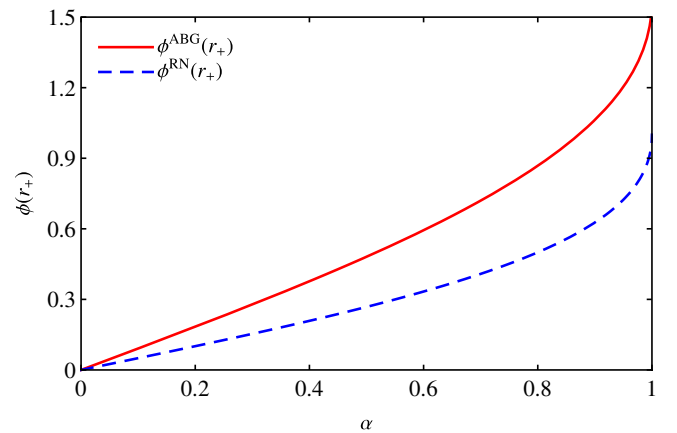

FIG. 3. Electrostatic potential at the event horizon, $\phi_+ \equiv \phi(r_+)$, as a function of the normalized charge α, for ABG and RN BHs.

B. Absorption cross section

The ACS σ, for a plane-wave incident upon a spherically symmetric BH, can be expanded in partial waves as follows:

$$\sigma = \sum_{l=0}^{\infty} \sigma_l, \qquad (29)$$

where the partial ACS is

$$\sigma_l = \frac{\pi}{\kappa^2}(2l+1)(1 - |\mathcal{R}_{\omega l}|^2). \qquad (30)$$

Hence, using Eq. (26),

$$\sigma_l = \frac{\pi}{\kappa^3}(2l+1)(\omega - \omega_c)|\mathcal{T}_{\omega l}|^2. \qquad (31)$$

For superradiant modes (with $0 < \omega < \omega_c = q\phi_+$), σ_l takes negative values, as the wave is *amplified* rather than absorbed.

In the limit $\omega \to \mu$ (from above), the momentum of the wave tends to zero, $\kappa \to 0$. Hence σ_l in Eq. (31) will diverge in this limit, unless $\lim_{\omega \to \mu} |\mathcal{T}_{\omega l}|^2/\kappa^3$ exists. In other words, σ_l will diverge unless the transmission factor $|\mathcal{T}_{\omega l}|^2$ approaches zero at least as rapidly as the cube of the momentum, κ^3. We will call the divergent case "unbounded" and the finite case "bounded."

It is clear that there are four possibilities to consider in the limit $\omega \to \mu$, namely: (i) bounded absorption, (ii) bounded superradiance, (iii) unbounded absorption, and (iv) unbounded superradiance. Cases (i)–(iii) have been observed in absorption by a RN (irregular) BH [58]. The fourth possibility, unbounded superradiance, does not appear to occur for RN BHs, but it does arise for the regular ABG BH, as we demonstrate in Sec. IV. To understand why this arises, we now turn attention to the properties of the potential.

C. The parameter space

In this section, we argue that it is possible to divide the parameter space into regions where behaviors (i)–(iv) occur (see above) by examining the behavior of an effective potential function. Considering Eq. (23) in the limit $\mu \to \omega$, we define

$$U(r) \equiv -V(r)|_{\mu=\omega},$$
$$= (\mu - q\phi(r))^2 - f(r)\left[\mu^2 + \frac{1}{r}\frac{df(r)}{dr} + \frac{l(l+1)}{r^2}\right]. \qquad (32)$$

In Fig. 4, we present the typical behavior of the function $U(r)$ in the ABG RBH spacetime. In the region where $U(r)$ is positive, the wave is propagative. The plot makes it clear that the existence of a propagative region extending to spatial infinity depends critically on the parameter values.

For the *uncharged* massive scalar field case, Jung and Park [83] defined the critical case as that in which the local
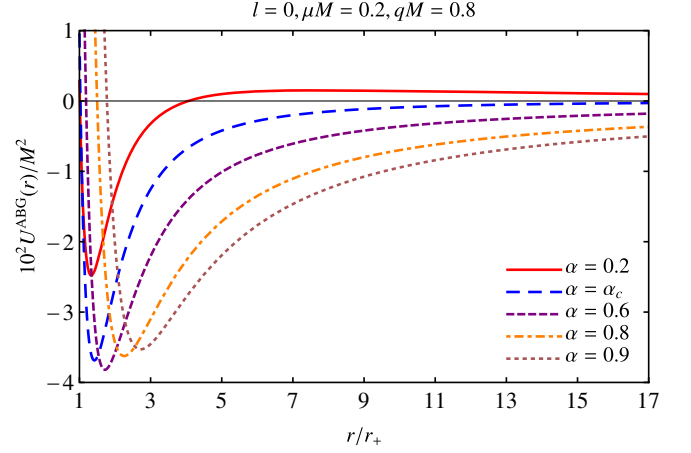

$$l = 0, \mu M = 0.2, qM = 0.8$$

FIG. 4. The function $U(r)$ of charged massive scalar waves in the background of the ABG RBH, as a function of r/r_+, considering $l = 0$, $\mu M = 0.2$, and $qM = 0.8$ for distinct values of α. In this case, superradiance occurs whenever $\alpha > 0.2702 = \alpha_c$.

maximum of $U(r)$ is exactly zero. This idea extends naturally to absorption of a charged field: the critical case is shown as the blue dashed line in Fig. 4, and this case defines a critical charge α_c (for fixed l, μM, and qM). For $\alpha < \alpha_c$, a propagative region extends from a certain radius r_c out to infinity [i.e., the region $r \in (r_c, \infty)$], whereas for $\alpha > \alpha_c$, the only propagative region is close to the horizon. It is natural to anticipate qualitatively different absorption properties in the limit $\omega \to \mu$, with the former (latter) case corresponding to unbounded (bounded) behavior.

In fact, to determine the existence of a propagative region that extends to infinity, it is sufficient to examine the large-r expansion of $U(r)$, given by

$$U(r) = 2\mu\frac{(\mu M - qQ)}{r} + \mathcal{O}(r^{-2}). \qquad (33)$$

At leading order, the expansion is identical for the RN and ABG BHs (as one might expect in the weak-field/linear regime). For $\mu M > qQ$, Newtonian attraction dominates over the Coulomb repulsion and the propagative region exists; for $\mu M < qQ$, Coulomb repulsion is dominant and the propagative region does not exist. The critical case is at $\mu M = qQ$.

We can now divide the parameter space into regions using two separatrices: $\mu M = qQ$ (the bounded/unbounded boundary) and $\mu = q\phi_+$ (the absorption/amplification boundary).

Figure 5 shows the anticipated behavior of the ACS in the limit $\omega \to \mu$ (i.e., $\kappa \to 0$), in the parameter space. The horizontal blue line ($\mu M = qQ$) separates the bounded and unbounded regions. The solid red line demarcates the onset of superradiance. In the RN case, there is no overlap between the unbounded and superradiant regions (though the boundaries meet in the extremal case, $Q = M$). This is consistent with an observed absence of unbounded

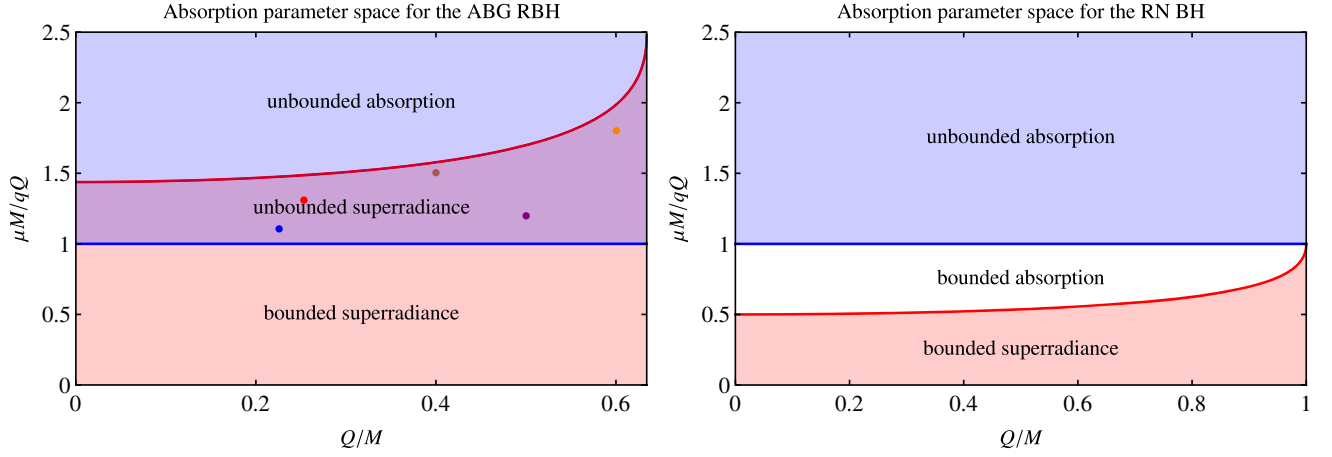FIG. 5. Absorption parameter space for ABG (left) and RN (right) BHs, as functions of Q/M. The solid red curve corresponds to the superradiance threshold and the solid blue curve to the attractive/repulsive threshold in Eq. (33). Left: the red line meets the vertical axis at $\mu M/qQ = 23/16$. The points highlight situations in which we have unbounded superradiance. The total ACS corresponding to these situations is exhibited in Fig. 10.

superradiance. Conversely, for the ABG BH, the superradiant region is significantly larger than in the RN case (even for $Q \to 0$), due to the increase in ϕ_+ (see Fig. 3). Consequently, the unbounded region overlaps with the superradiant region, and hence we should anticipate unbounded superradiance (that is, unbounded amplification) to occur in the limit $\omega \to \mu$, in this region of the parameter space. These conclusions are supported by the numerical evidence presented in Sec. IV C.

D. High-frequency approximation

We now turn our attention to absorption in the regime of high frequencies and short wavelengths. In this regime, the characteristics of the charged massive scalar wave can be associated with the trajectories of charged particles subject to the Lorentz force imparted by the electric background field. In order to obtain the equations of motion associated with our problem, we consider the following Lagrangian:

$$\mathrm{L_{cp}} = \frac{1}{2} g_{\mu\nu} \dot{x}^\mu \dot{x}^\nu + \frac{q_{cp}}{m} A_\mu \dot{x}^\mu, \quad (34)$$

where the overdot stands for the derivative with respect to the proper time, and q_{cp} and m are the charge of the particle and mass of the particle, respectively. From Eq. (34), one can introduce the conserved quantities

$$E = m \frac{\partial \mathrm{L_{cp}}}{\partial \dot{t}}, \quad (35)$$

$$L = -m \frac{\partial \mathrm{L_{cp}}}{\partial \dot{\varphi}}, \quad (36)$$

which are related to the energy and the angular momentum of the particle and, in the semiclassical limit, are associated with ω and $l + 1/2$, respectively. Using Eqs. (34)–(36) together with $g_{\mu\nu} \dot{x}^\mu \dot{x}^\nu = 1$ (the condition that a massive

particle follows a timelike path, parametrized by its proper time [84]), one can show that

$$\dot{r}^2 \left(\frac{m^2}{L^2} \right) = \frac{(E - q_{cp} A_0)^2}{L^2} - f(r) \left(\frac{m^2}{L^2} + \frac{1}{r^2} \right), \quad (37)$$

in which, due to the spherical symmetry, we considered the motion in the equatorial plane ($\theta = \pi/2$).

By defining the impact parameter $b \equiv L/vE$ and $\mathcal{K}(r) \equiv \dot{r}^2 (m^2/L^2)$, we can rewrite Eq. (34) as

$$\mathcal{K}(r) = \frac{1}{b^2 v^2} \left(1 - \sqrt{1 - v^2} \frac{q_{cp}}{m} A_0(r) \right)^2 - f(r) \left(\frac{1 - v^2}{b^2 v^2} + \frac{1}{r^2} \right), \quad (38)$$

where v is a dimensionless parameter defined by

$$v \equiv \sqrt{1 - \frac{m^2}{E^2}}. \quad (39)$$

Since we are interested in the unbounded timelike paths, i.e., $\kappa > 0$, this parameter is limited by $0 < v \leq 1$. Considering that $\mathcal{K}(r)$ and its first derivative vanish at the critical radius r_c, namely,

$$\mathcal{K}(r_c) = 0, \quad (40)$$

$$\frac{d\mathcal{K}(r_c)}{dr} = 0, \quad (41)$$

we may find the critical impact parameter b_c,

$$b_c^2 = \frac{r_c^2}{m^2 v^2 f(r_c)} [m^2 (1 + (v^2 - 1) f(r_c)) + q_{cp} A_0(r_c)(q_{cp} A_0(r_c)(1 - v^2) - 2m\sqrt{1 - v^2})], \quad (42)$$

and an equation that gives the values of r_c,

$$\frac{2f(r_c)(m^2 z f(r_c) - (m - q_{\rm cp}\sqrt{z}A_0(r_c))(m - q_{\rm cp}\sqrt{z}(r_c A_0'(r_c) + A_0(r_c)))) + r_c f'(r_c)(m - q_{\rm cp}\sqrt{z}A_0(r_c))^2}{m^2 z f(r_c) - (m - q_{\rm cp}\sqrt{z}A_0(r_c))^2} = 0, \quad (43)$$

where we defined $z \equiv 1 - v^2$ and the prime (′) denotes derivative with respect to the radial coordinate r. For $q_{\rm cp} = 0$, we recover the b_c and r_c of the massive chargeless case, which are given by [69]

$$b_c^2 = \frac{r_c^2(1 + (v^2 - 1)f(r_c))}{v^2 f(r_c)}, \quad (44)$$

$$2(1 + (v^2 - 1)f(r_c)) = r_c \frac{f'(r_c)}{f(r_c)}, \quad (45)$$

respectively. In the limit $m \to 0$, which implies in $v \to 1$, we obtain the results for the massless case [78]. The high-frequency absorption cross section, also called geometric cross section (GCS), $\sigma_{\rm gcs}$, is given by [84]

$$\sigma_{\rm gcs} = \pi b_c^2. \quad (46)$$

IV. RESULTS

A. Numerical analysis

We can obtain the reflection and transmission coefficients, given by Eqs. (25), by numerically integrating Eq. (22) from very close to r_+ up to far from the BH, with the boundary conditions given by Eqs. (24) and their derivatives. Then we compute the total ACS using Eq. (29). The oscillatory character of the ACS is related to the partial waves contributions [see Eq. (30)]. We have chosen, in general, to perform the summation in Eq. (29) up to $l = 20$.
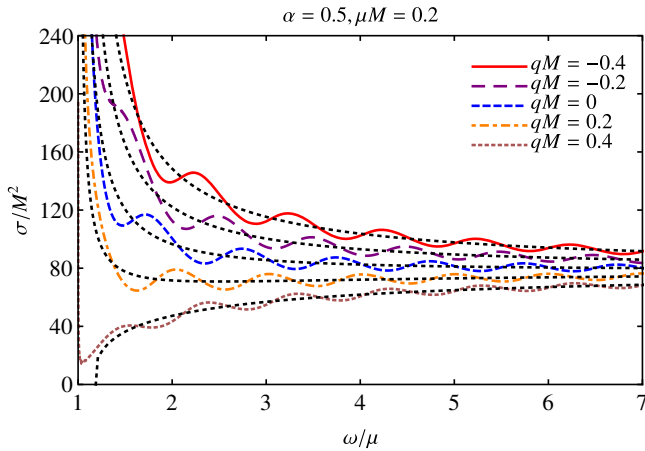
The GCS is obtained numerically through Eq. (46), using Eqs. (42) and (43).

B. ABG regular black hole cross sections

Figures 6 and 7 show the total ACS for different values of the charge (qM) and mass (μM) couplings, respectively. Generically, we can see that the total ACS oscillates around the GCS (black dotted lines), with good agreement in the high-frequency regime. Moreover, for a fixed value of μM and α, we observe that the absorption increases (diminishes) as we consider smaller (higher) values of qQ, as a consequence of the Lorentz force. As shown in Fig. 7, the total ACS increases as we increase μM, so that the increase of μM leads to a higher absorption of planar scalar waves. For massive planar scalar waves, the effective potential typically admits an (inner) local maximum and an (outer) local minimum; as we increase μM, the stationary points move closer together and the maximum of the potential decreases, until the stationary points eventually merge and the potential barrier vanishes. Hence, increasing μM leads to strongly absorbed unbounded modes, similar to the RN BH case [69].

Figure 8 shows the total ACS together with the partial ACS for two choices of qM, with the normalized BH charge $\alpha = 0.5$ and the field mass coupling $\mu M = 0.2$. The plots show that the oscillatory pattern in the total ACS is related to the sequential contributions from partial ACSs $l = 0, 1, 2, \ldots$. The monopole ($l = 0$) dominates the behavior of the total ACS in the low-frequency regime. Note that, although the values of α and μM are equal in both panels of
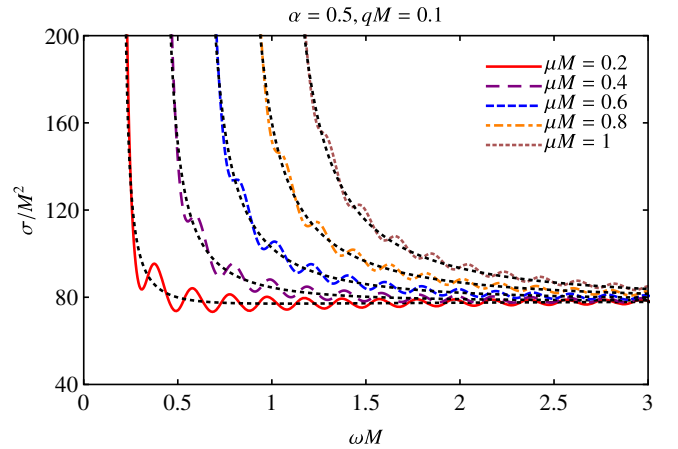

FIG. 6. Total ACS of charged massive scalar waves in the background of the ABG RBH, as a function of ω/μ, for different choices of qM, considering $\alpha = 0.5$ and $\mu M = 0.2$. The ACS is compared with the geometric cross section (dashed black lines).

FIG. 7. Total ACS of charged massive scalar waves in the background of the ABG RBH, as a function of ωM for $\alpha = 0.5$, $qM = 0.1$, and different values of μM.
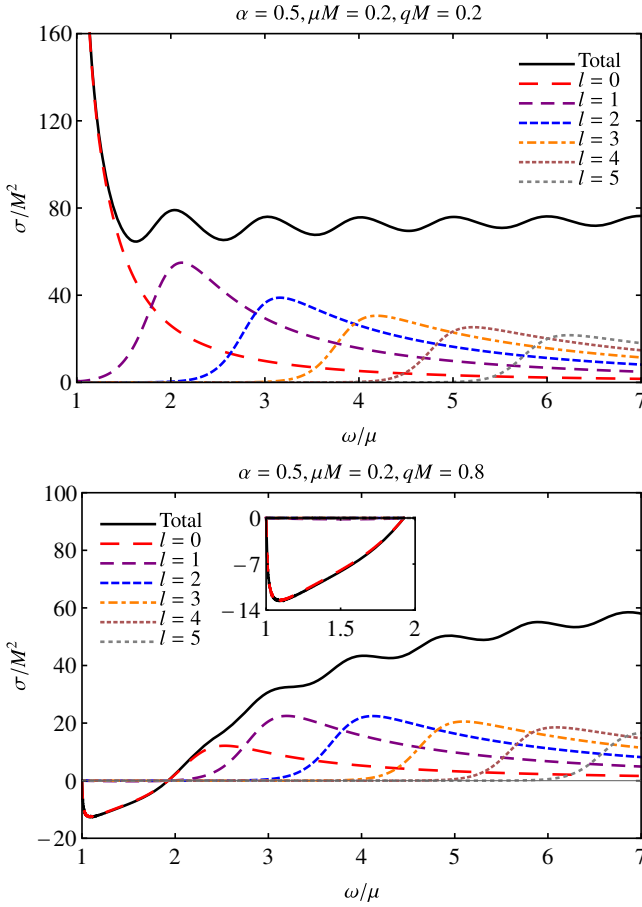
FIG. 8. Partial and total ACSs of charged massive scalar waves in the background of the ABG RBH, as functions of ω/μ, for $\alpha = 0.5$ and $\mu M = 0.2$, in two distinct scenarios: (top) $qM = 0.2$ and (bottom) $qM = 0.8$. The inset in the bottom panel emphasizes superradiance that occurs for $1 < \omega/\mu \lesssim 1.924$.

Fig. 8, superradiance occurs only in the bottom panel case. We observe that the ACS is *negative* in the range $\mu < \omega \lesssim 2\mu$. Physically, a negative cross section implies that the stimulation from the plane wave causes the BH to transmit mass-energy and charge into the field.

In Fig. 9, we present the amplification factor of massive charged scalar fields in the background of an ABG RBH. [We exhibit the amplification factor (27) in percentage, i.e., $Z_{\omega l}[\%] \equiv 100 Z_{\omega l}$, and restricted to the regions where $Z_{\omega l}[\%] \geq 0$]. As we can see, the maximum superradiant amplification increases with the charge of the scalar field, for fixed values of the BH mass and (positive) charge.

C. Unbounded superradiance from a regular ABG black hole

In the previous section, we presented some typical absorption properties of charged massive scalar waves in the background of the ABG RBH. In the limit $\omega \to \mu$ we saw two types of behavior: unbounded absorption (Figs. 6–8, upper plot) and bounded superradiance
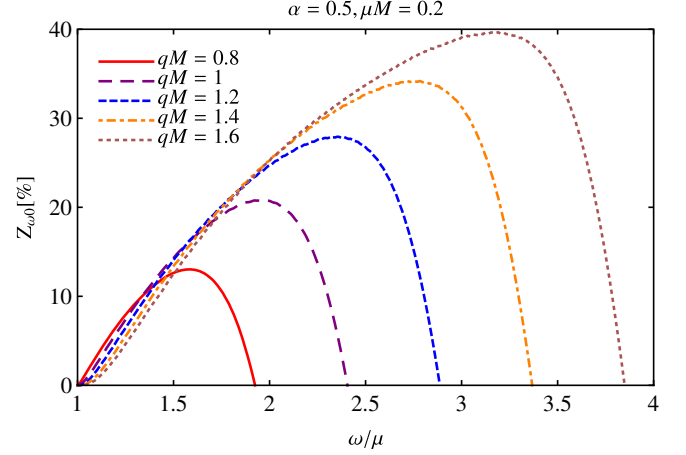

FIG. 9. Superradiant amplification of massive charged scalar fields by an ABG RBH with $\alpha = 0.5$, as a function of ω/μ. Here we consider the mode $l = 0$, $\mu M = 0.2$, and distinct values of qM.

(Fig. 8, lower plot). In this section, we show that the ABG RBH can also display unbounded superradiance for parameter choices informed by Fig. 5 and the discussion in Sec. III C.

Figure 10 shows the ACS of the ABG RBH for a selection of parameter choices (informed by Fig. 5) for which we would expect to see unbounded superradiance. As we can see, the results are consistent with the expectations of Fig. 5: in all cases, the cross section σ is negative (indicating superradiant amplification) and it grows without bound as $\omega \to \mu$.

The results in Fig. 10 reveal a remarkable implication of the electromagnetic fields associated with (electrically charged) NED-based RBH geometries: they generate a superradiant divergence in the ACS of a charged, massive scalar field. That is, an ABG BH stimulated by a massive plane wave of low momentum has an ACS that is unbounded
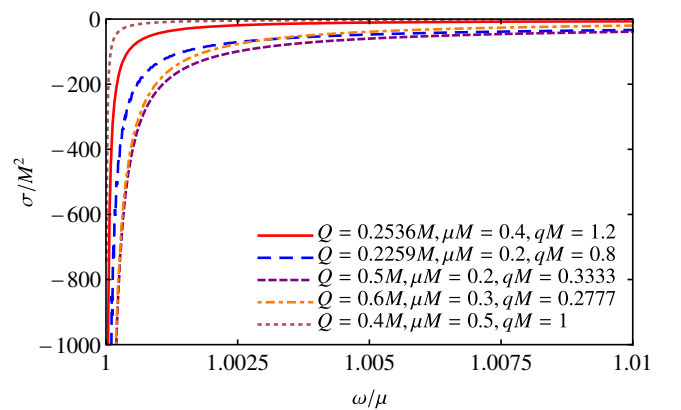

FIG. 10. Total ACS of charged massive scalar waves in the background of the ABG RBH, as a function of ω/μ, considering situations in which we have unbounded superradiance (the points in the left panel of Fig. 5). We focus on the region near the limit $\omega M \to \mu M$ to emphasize the divergent behavior of the total ACS in the superradiant regime.

from below. This is in stark contrast to the RN BH, where the cross section cannot obtain arbitrary negative values.

D. Comparison with the Reissner-Nordström BH

In this section, we compare the absorption properties of ABG RBHs with those of RN BHs [58].

Figure 11 shows a comparison between the total ACSs of ABG RBHs and RN BHs for $\alpha = 0.4$, $qM = 1.6$, and two values of μM. We see that, for a fixed value of μM, the total ACS of the ABG RBH is smaller than the total ACS of the RN BH, across the frequency range. We also observe that, for $\mu M = 0.4$, the ABG RBH exhibits superradiant scattering (i.e., $\sigma < 0$ in some range of ω), whereas the RN BH does not (for these parameters). This feature is due to the higher threshold frequency ($\omega_c = q\phi_+$) for superradiance in the ABG case [see Sec. III, in particular, Eq. (28) and Fig. 3] and the condition for unbounded modes, namely, $\omega^2 > \mu^2$. For $\mu M = 0.4$, both systems show unbounded absorption as $\omega \to \mu$. Conversely, for $\mu M = 0.8$, the RN shows bounded absorption, whereas the ABG RBH shows bounded super-radiance, in this limit.

Referring again to the parameter space shown in Fig. 5, in the RN BH case the unbounded region and the superradiant region of the parameter space are disjoint. Therefore, we do not expected to observe unbounded super-radiance (as $\omega \to \mu$) in the RN case. In this sense, absorption by the RN BH is qualitatively different to absorption by the ABG RBH, for which it is possible to find a set of field and RBH parameters that leads to unbounded superradiance (see Fig. 10). A further notable feature of Fig. 5 is that bounded absorption does not occur in the ABG case (since the bounded case is necessarily superradiant), whereas it does in the RN case; see Fig. 11 for an example.
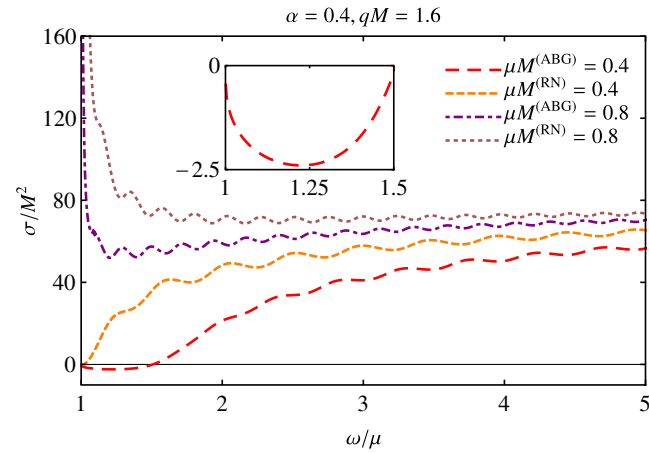
Figure 12 shows results for the ACSs in two distinct sets: (i) for $\alpha = 0.4$, $\mu M = 0.4$, and different values of qM (top panel); and (ii) for $\mu M = 0.2$, $qM = 0.4$, and different values of α (bottom panel). We note that, similar to the behavior presented in Fig. 11, for a given set of parameters, superradiance might occur only for the ABG RBH. We see again that the propagating waves are more absorbed in the RN case, when $qQ > 0$; however, for $qQ < 0$, we observe the opposite behavior.

Figure 13 compares the partial ACSs of ABG and RN BHs. In this case, for the chosen parameters we have superradiance for both BH types. The range of frequency in which $\sigma < 0$ is larger in the ABG case than in the RN case. The dominant contribution to superradiance comes from the monopole mode, $l = 0$.

A comparison of the amplification factors in the ABG and RN geometries is exhibited in Fig. 14. The superradiant amplification in the background of the ABG RBH, for the same values of α, μM, and qM, is typically larger than that in the corresponding RN geometry, in agreement with the results presented in Figs. 11–13.

FIG. 11. Comparison between the total ACSs of charged massive scalar waves in the background of ABG and RN BHs, as functions of ω/μ, considering $\alpha = 0.4$, $qM = 1.6$, and different choices of μM. Inset: highlights the range of frequency ($1 < \omega/\mu \lesssim 1.5$, for $\mu M^{(ABG)} = 0.4$) for which the ACS becomes negative, denoting superradiance.
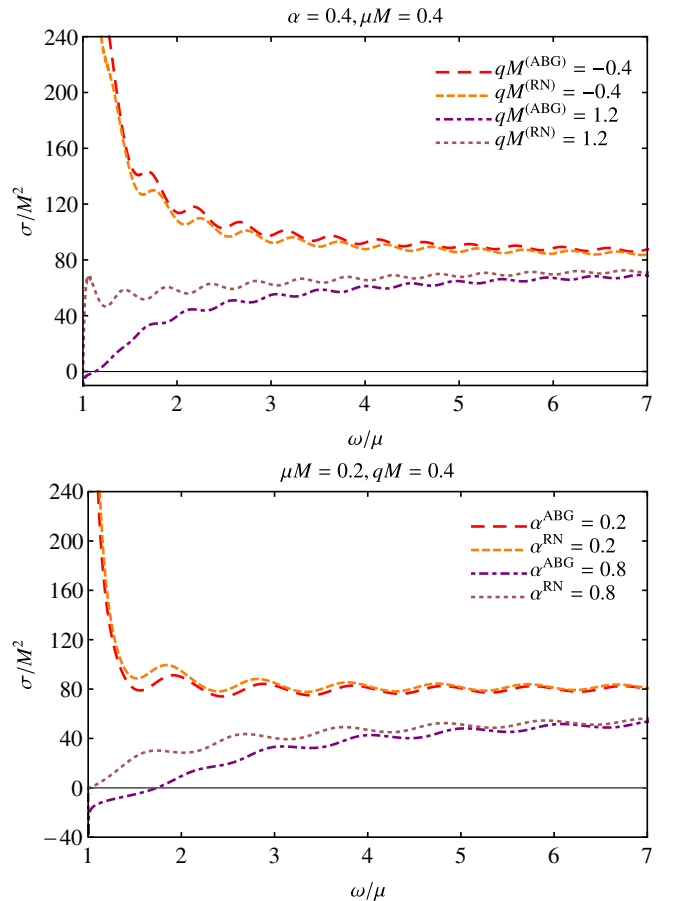
FIG. 12. Comparison between the total ACSs of charged massive scalar waves in the background of ABG and RN BHs, as functions of ω/μ, in two different scenarios: (i) for $\alpha = 0.4$, $\mu M = 0.4$, and different values of qM (top); and (ii) for $\mu M = 0.2$, $qM = 0.4$, and distinct values of α (bottom).
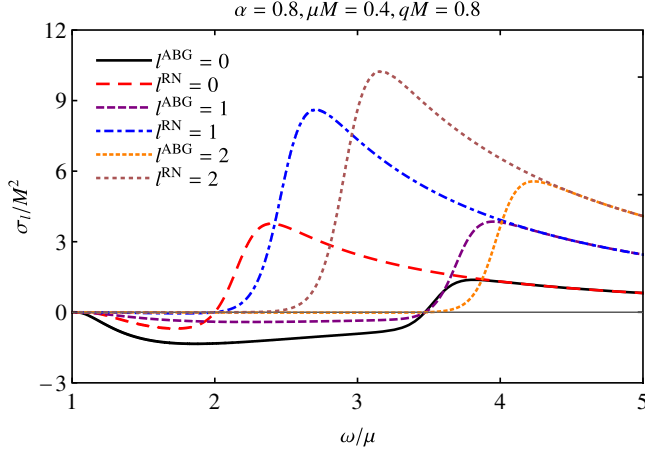
FIG. 13. Comparison between the partial ACSs of charged massive scalar waves in the background of ABG and RN BHs, as functions of ω/μ, with $\alpha = 0.8$, $\mu M = 0.4$, and $qM = 0.8$.

FIG. 15. Total ACSs of charged massive scalar waves for the pairs $(\alpha^{\mathrm{ABG}}, \alpha^{\mathrm{RN}}) = (0.2, 0.1794)$ and $(\alpha^{\mathrm{ABG}}, \alpha^{\mathrm{RN}}) = (0.5, 0.4498)$ as functions of ω/μ. In both cases, we set $\mu M = 0.6$ and $qM = 0.2$.

We end this section by noting that all results presented here, as well as those not shown, are consistent with the parameter space for ABG and RN BHs introduced in Fig. 5.

E. Mimic configurations

In this section, we show that it is possible to find combinations of the normalized charge of the BH solution, and the parameters (charge and mass) of the scalar field such that the ACSs of ABG and RN BHs are very similar. We start by computing the values of α for which the GCS (see Sec. III D) of the ABG RBH is equal to that of the RN BH, for fixed values of the charged massive particle parameters EM, $q_{cp}M$, and mM. Next, we compute the ACSs using the corresponding values of α, qM, and μM.

Figure 15 shows the total ACSs for specific pairs $(\alpha^{\mathrm{ABG}}, \alpha^{\mathrm{RN}})$ with $\mu M = 0.6$ and $qM = 0.2$. As we can

see, the total ACSs of the two types of BHs (regular ABG and irregular RN) can be very similar in the middle- to high-frequency range, particularly for low-to-moderate values of α, but distinguishable in the low-frequency regime.

Figure 16 shows that, for a neutral field ($qM = 0$), the ACSs of the two types of BHs can be very similar across the whole frequency range, particularly for small-to-moderate values of α. Here we consider two pairs of choices of $(\alpha^{\mathrm{ABG}}, \alpha^{\mathrm{RN}})$ that lead to the same GCS. The field charge q increases the differences between the absorption pattern of ABG and RN BHs, particularly at lower frequencies.

It is possible to find configurations for which a massive and charged scalar field has the same value of the critical frequency ω_c of superradiance in the two spacetimes, that is,
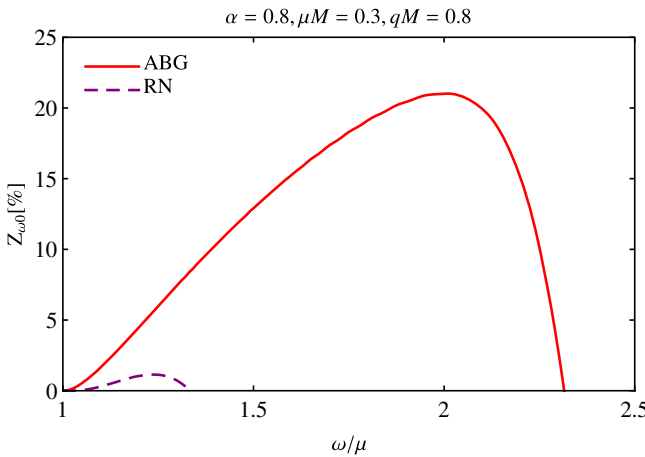

FIG. 14. Superradiant amplification of charged massive scalar fields by ABG and RN BHs, as a function of ω/μ. Here we consider $\alpha = 0.8$, $l = 0$, $\mu M = 0.3$, and $qM = 0.8$ in both geometries.
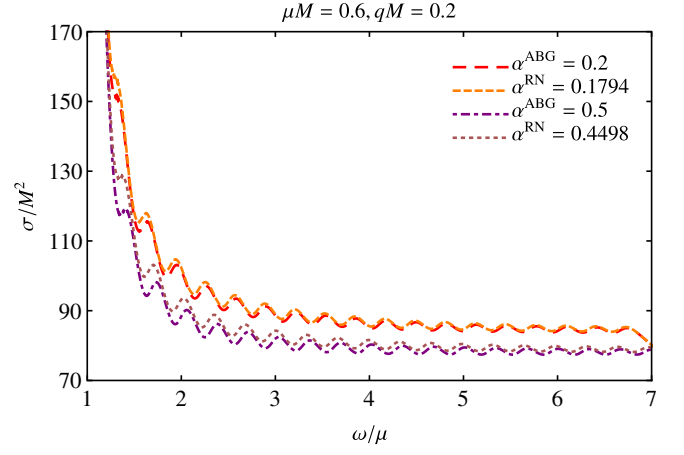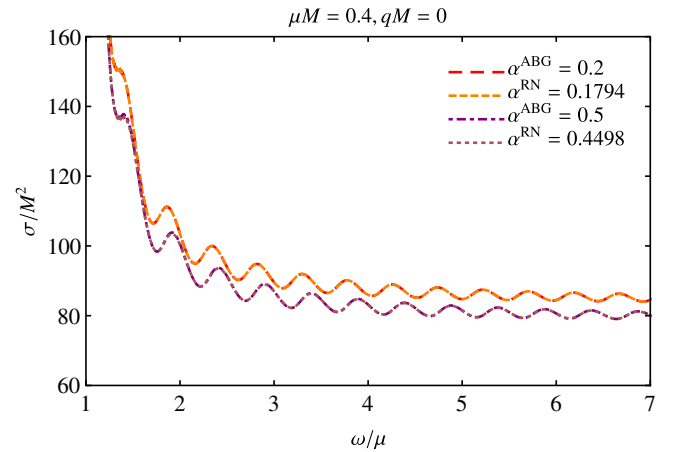

FIG. 16. Total ACSs of charged massive scalar fields for the pairs $(\alpha^{\mathrm{ABG}}, \alpha^{\mathrm{RN}}) = (0.2, 0.1794)$ and $(\alpha^{\mathrm{ABG}}, \alpha^{\mathrm{RN}}) = (0.5, 0.4498)$, as functions of ω/μ. In both cases, we set $\mu M = 0.4$ and $qM = 0$.

FIG. 19. Total ACS for $qM = 1$ and $\mu M = 0.2$ in the ABG geometry and for $qM = 1.4$ and $\mu M = 0.4$ in the RN spacetime. Superradiance occurs when $\omega M < \omega_c M = 0.7$ in both scenarios.
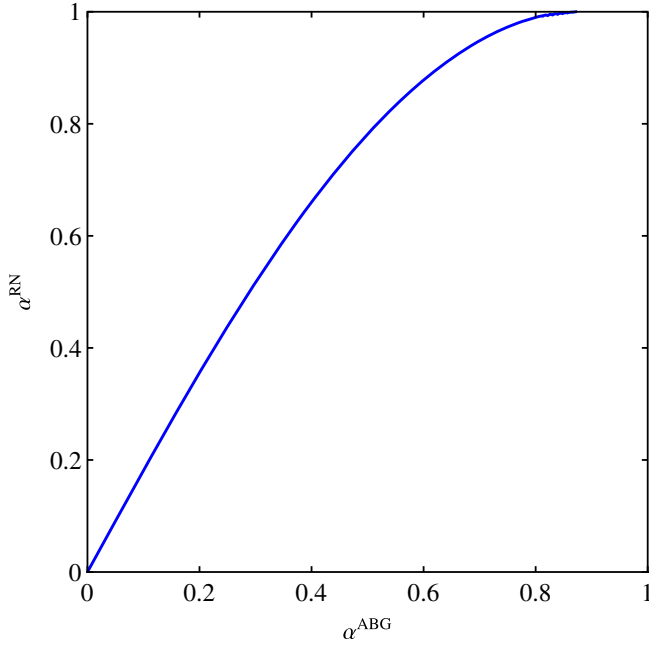
FIG. 17. Values of the pair $(\alpha^{ABG}, \alpha^{RN})$ for which a fixed choice of qM presents the same critical frequency in the background of ABG and RN BHs.

$$\omega_c^{ABG} = \omega_c^{RN}. \tag{47}$$

Figure 17 shows the values of the pair $(\alpha^{ABG}, \alpha^{RN})$ for which the critical frequency is the same in both backgrounds, considering a fixed value of qM. These configurations can be found up to $\alpha^{ABG} \lesssim 0.8716$.

Figure 18 shows the total ACS for pairs $(\alpha^{ABG}, \alpha^{RN})$ with the same critical frequency ω_c. We see that the

effect of superradiance is enhanced in the ABG case, as one would expect given the stronger amplification shown in Fig. 14.

It is also possible to find situations in which scalar fields with different masses and charges have the same critical frequency ω_c in the background of ABG and RN BH spacetimes. In Fig. 19, we consider a scalar field with $qM = 1$ and $\mu M = 0.2$ in the ABG spacetime and a scalar field with $qM = 1.4$ and $\mu M = 0.4$ in the RN geometry. As we can see, the distinct scalar fields are superradiantly scattered whenever $\omega M < 0.7$. Figure 20 shows the amplification factors for the same parameters, highlighting once again that superradiance amplification is enhanced for the ABG BH relative to the RN BH.
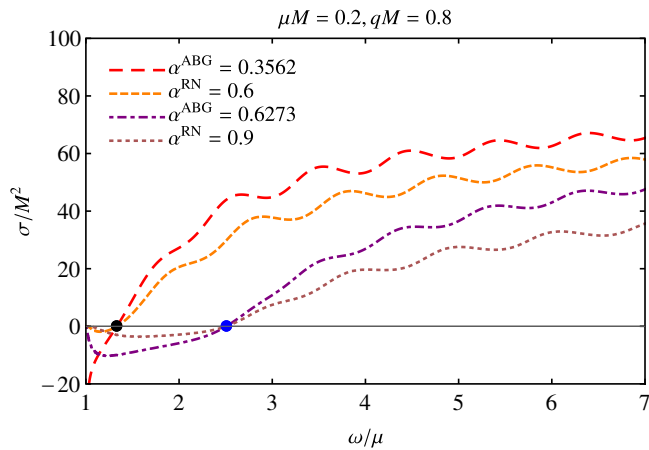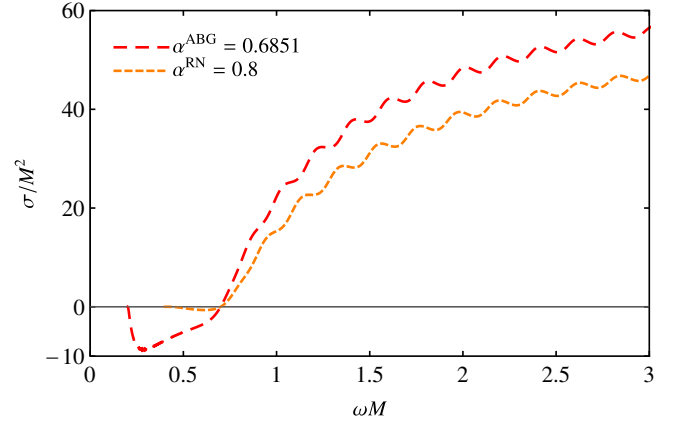

FIG. 18. Example of situations in which a massive and charged scalar field presents the same critical frequency in the background of ABG and RN BHs. The small disks denote the values of the critical frequency, namely, $\omega_c = 1.3333$ (left disk) and $\omega_c = 2.5071$ (right disk).
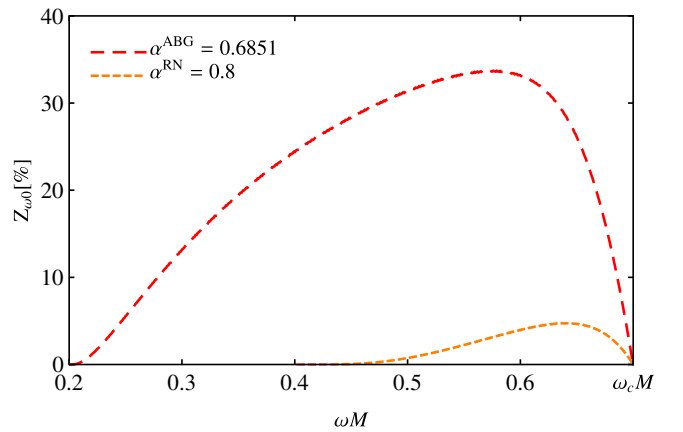

FIG. 20. Superradiant amplification of massive charged scalar fields, as a function of ωM, considering the same parameters used in Fig. 19, for which the critical frequency is $\omega_c M = 0.7$.

V. CONCLUDING REMARKS

Within GR, the standard BH solutions (Schwarzschild, Reissner-Nordström, Kerr, and Kerr-Newman) possess a common feature in their core: a curvature singularity hidden by an event horizon. On the other hand, certain *regular* BH solutions, i.e., objects with an event horizon but with no curvature singularity, can be obtained by minimally coupling NED models to GR. Much work is underway to determine the properties of RBHs. Contributing to this effort, we have scrutinized the absorption properties of charged massive scalar fields in the background of the electrically charged RBH solution proposed by Ayón-Beato and García [18].

The most intriguing result of our study is that regular ABG BHs, unlike their RN counterparts, exhibit unbounded superradiance (as $\omega \to \mu$) in massive scalar fields, within a certain parameter range. More precisely, the cross section σ is unbounded from below as $\omega \to \mu$; this is shown clearly in Fig. 10. The region of parameter space in which unbounded superradiance occurs is clarified in Sec. III C and Fig. 5.

Some care is needed in interpreting the physical meaning of the divergence of the cross section σ as $\omega \to \mu$. In the particle picture, a divergence arises naturally because particles of low momentum and large impact parameters are attracted by the BH, with $b_c \to \infty$ as $\kappa \to 0$. In the wave picture, a divergence in σ arises if the transmission factor does not go to zero as rapidly as the cube of the momentum κ in the denominator of Eq. (31); and if this occurs in the superradiant regime $\omega < \omega_c$, then the unbounded superradiance phenomenon occurs. Notably, the amplification factor, $Z_{\omega l}$ in Eq. (27), does *not* diverge in our numerical results.

In principle then, by stimulating the BH with a planar wave of low momentum ($\kappa \to 0$) in a massive charged field, one can extract (via superradiance) unbounded quantities of mass and charge from the ABG BH (within the limitations of the linearized regime of weak scalar fields). It is important to stress, however, that the divergence in σ is related to the fact that the BH is interacting with a planar wave of infinite lateral extent (and $b_c \to \infty$ as $\kappa \to 0$). Therefore, one should not expect unbounded extraction of energy to be possible (even in principle) for a stimulating wave of finite width and duration.

Some further interesting aspects of the ACS are summarized below:

(i) Massive scalar waves are typically more absorbed than massless ones, and absorption increases with the value of μM. This result is expected since larger field masses lead to larger GCSs, and large field masses are associated with strongly absorbed modes [69,83].

(ii) In the case of a charged scalar field, due to the Lorentz force, the absorption for $qQ < 0$ is typically larger than for $qQ > 0$.

(iii) Low-frequency waves satisfying the condition $\omega < \omega_c$ [cf. Eq. (28)] can have a *negative* ACS. This occurs due to the superradiant amplification of low multipoles of the field (principally, in the $l = 0$ mode) [55].

(iv) The absorption of scalar waves by ABG RBHs is typically larger than for RN BHs (for equivalent q, M, and α), when the value of the charge coupling qQ is negative. Conversely, $\sigma^{\mathrm{RN}} > \sigma^{\mathrm{ABG}}$ when $qQ > 0$.

(v) The critical superradiant frequency of the ABG BH is always larger than that of the RN BH, for equivalent parameters. Moreover, superradiant amplification is stronger for the ABG BH. Both aspects are due to the enhanced electrostatic potential at the horizon, ϕ_+, in the ABG case (i.e., $\phi_+^{\mathrm{ABG}} > \phi_+^{\mathrm{RN}}$).

We showed in Sec. IV E that, for certain parameter choices, the ABG RBH solution can mimic the RN solution, from the point of view of absorption spectrum, reinforcing the results presented in Refs. [78,81]. It is also possible to find configurations for which scalar fields with different masses and charges, in the background of ABG and RN BHs, have the same critical superradiant frequency.

Several avenues for further investigation are open. First, we note that superradiant scattering is, in some sense, the wave analog of the Penrose process. In light of the results here, it could be worth studying the Penrose process for the ABG BH in detail; that is, the scenario of a charged particle, incident from infinity, that splits into two parts in the vicinity of the BH, with one part ejected to infinity and the other absorbed.[2] In a Penrose process, the escaping particle has *more* mass-energy than the incident one. It would be interesting to compare the regions of parameter space in which energy extraction can occur, again drawing a comparison between the RN BH and the ABG BH.

Second, the existence of the unbounded superradiance region in Fig. 5 strongly hints at the existence of superradiantly unstable quasibound states in the spectrum of the massive charged scalar field on the ABG spacetime. Previous investigations on the RN spacetime have suggested that it is *not* possible to form quasibound states that are also superradiant in the RN case. Heuristically, the reason is clear: for bound states one needs an *attractive* potential in the far field, which necessitates $\mu M > qQ$; then modes with $\omega < \mu$ do not lie in the superradiant regime $\omega < q\phi_+^{\mathrm{RN}} = qQ/r_+$ of the RN BH. Conversely, as shown in Fig. 5, modes satisfying $\mu M/qQ > 1$ *can* also be superradiant on the ABG spacetime, due to the increase in the electric potential at the horizon, ϕ_+. This implies that certain quasibound modes of the massive charged scalar field will grow exponentially with time and thus that the ABG BH suffers a superradiant instability. This is under active investigation [86].

---

[2]In Ref. [85], the authors studied the Penrose process in the ABG RBH, but considered neutral particles.

Third, the ABG BH is just one example in the regular class in NED. It would be interesting to clarify whether other solutions in this class also exhibit a stronger electromagnetic field at the horizon and thus an enhanced region of superradiance with associated phenomena, or whether the ABG BH stands alone in this respect.

Finally, real astrophysical BHs are known to be rotating. Future studies of absorption by spinning RBHs would clarify the interplay between charged superradiance (studied here) and rotational superradiance.

We conclude this paper by discussing some potential observational impacts. In recent years, the EHT Consortium has provided the first images of the shadows of the supermassive BHs M87* [5] and Sgr A* [87]. In principle, observations of BH shadows probe the geometry of the spacetime near the light ring, and thus there should be observable differences between regular and singular BHs, as well as between the charged and uncharged scenarios. The area of the shadow is closely linked to the ACS in the high-frequency limit, that is, to the geometric capture cross section σ_{gcs} [see Eq. (46)]. This is influenced by the charge of the spacetime and by its causal structure, but we do not expect σ_{gcs} to be significantly affected by unbounded superradiance. However, unbounded superradiance may provide an efficient mechanism for the BH to deplete its charge (in addition to the Schwinger effect) and, moreover, a superradiant instability in the same region of the parameter space could lead to the formation of a scalar field cloud, with its own observational signatures. Another arena to explore is the effect of charge and NED on gravitational waves from

two-body coalescences; for instance, using the merger-ringdown signal for charged BHs, one may seek to constrain the charges of the progenitors and the product of the merger [88]. In certain astrophysical scenarios, scalar fields are used to model dark matter candidates (see Ref. [89] and references therein), and dark matter models can support a small amount of charge [90] (though several orders lower than that of an electron). Further study is still needed to understand the role of superradiant scattering in such scenarios, including on RBH spacetimes.

ACKNOWLEDGMENTS

[1] C. M. Will, The confrontation between general relativity and experiment, Living Rev. Relativity **17,** 4 (2014).

[2] L. C. B. Crispino and D. Kennefick, A hundred years of the first experimental test of general relativity, Nat. Phys. **15,** 416 (2019).

[3] L. C. B. Crispino and S. Paolantonio, The first attempts to measure light deflection by the Sun, Nat. Astron. **4,** 6 (2020).

[4] B. P. Abbott *et al.* (LIGO Scientific and Virgo Collaborations), Observation of gravitational waves from a binary black hole merger, Phys. Rev. Lett. **116,** 061102 (2016).

[5] K. Akiyama *et al.* (Event Horizon Telescope Collaboration), First M87 Event Horizon Telescope results. I. The shadow of the supermassive black hole, Atrophys. J. **875,** L1 (2019).

[6] R. Narayan and J. E. McClintock, Observational evidence for black holes, arXiv:1312.6698.

[7] J. Kormendy and L. C. Ho, Coevolution (or not) of supermassive black holes and host galaxies, Annu. Rev. Astron. Astrophys. **51,** 511 (2013).

[8] A. M. Ghez, B. L. Klein, M. Morris, and E. E. Becklin, High proper-motion stars in the vicinity of Sagittarius A*:

Evidence for a supermassive black hole at the center of our Galaxy, Astrophys. J. **509,** 678 (1998).

[9] A. M. Ghez *et al.*, Measuring distance and properties of the Milky Way's central supermassive black hole with stellar orbits, Astrophys. J. **689,** 1044 (2008).

[10] M. Heusler, *Black Hole Uniqueness Theorems* (Cambridge University Press, Cambridge, England, 1996).

[11] R. Penrose, "Golden Oldie": Gravitational collapse: The role of general relativity, Gen. Relativ. Gravit. **34,** 1141 (2002).

[12] S. W. Hawking and G. F. R. Ellis, *The Large Scale Structure of Space-Time* (Cambridge University Press, Cambridge, England, 1973).

[13] J. Bardeen, Non-singular general relativistic gravitational collapse, *Proceedings of the International Conference GR5, Tbilisi, U.S.S.R., 1968* (unpublished).

[14] A. Borde, Open and closed universes, initial singularities, and inflation, Phys. Rev. D **50,** 3692 (1994).

[15] C. Barrabès and V. P. Frolov, How many new worlds are inside a black hole?, Phys. Rev. D **53,** 3215 (1996).

[16] M. Mars, M. M. Martín-Prats, and J. M. M. Senovilla, Models of regular Schwarzschild black holes satisfying weak energy conditions, Classical Quantum Gravity **13**, L51 (1996).

[17] A. Cabo and E. Ayón-Beato, About black holes with nontrapping interior, Int. J. Mod. Phys. A **14**, 2013 (1999).

[18] E. Ayón-Beato and A. García, Regular black hole in general relativity coupled to nonlinear electrodynamics, Phys. Rev. Lett. **80**, 5056 (1998).

[19] M. Born, On the quantum theory of the electromagnetic field, Proc. R. Soc. A **143**, 410 (1934).

[20] M. Born and L. Infeld, Foundations of the new field theory, Proc. R. Soc. A **144**, 425 (1934).

[21] J. F. Plebański, *Lectures on Non-Linear Electrodynamics* (NORDITA, Copenhagen, Denmark, 1970).

[22] S. A. Gutiérrez, A. L. Dudley, and J. F. Plebański, Signals and discontinuities in general relativistic nonlinear electrodynamics, J. Math. Phys. (N.Y.) **22**, 2835 (1981).

[23] W. Heisenberg and H. Euler, Folgerungen aus der Diracschen Theorie des Positrons, Z. Phys. **98**, 714 (1936).

[24] E. S. Fradkin and A. A. Tseytlin, Non-linear electrodynamics from quantized strings, Phys. Lett. **163B**, 123 (1985).

[25] N. Seiberg and E. Witten, String theory and noncommutative geometry, J. High Energy Phys. 09 (1999) 032.

[26] A. A. Tseytlin, Born-Infeld action, supersymmetry and string theory, arXiv:hep-th/9908105.

[27] M. Novello, S. E. Perez Bergliaffa, and J. Salim, Nonlinear electrodynamics and the acceleration of the Universe, Phys. Rev. D **69**, 127301 (2004).

[28] R. P. Mignani, V. Testa, D. González Caniulef, R. Taverna, R. Turolla, S. Zane, and K. Wu, Evidence for vacuum birefringence from the first optical-polarimetry measurement of the isolated neutron star RX J1856.5-3754, Mon. Not. R. Astron. Soc. **465**, 492 (2017).

[29] M. Aaboud *et al.* (ATLAS Collaboration), Evidence for light-by-light scattering in heavy-ion collisions with the ATLAS detector at the LHC, Nat. Phys. **13**, 852 (2017).

[30] G. Aad *et al.* (ATLAS Collaboration), Observation of light-by-light scattering in ultraperipheral $Pb + Pb$ collisions with the ATLAS detector, Phys. Rev. Lett. **123**, 052001 (2019).

[31] A. Ejlli, F. Della Valle, U. Gastaldi, G. Messineo, R. Pengo, G. Ruoso, and G. Zavattini, The PVLAS experiment: A 25 year effort to measure vacuum magnetic birefringence, Phys. Rep. **871**, 1 (2020).

[32] D. Delphenich, Nonlinear electrodynamics and QED, arXiv:hep-th/0309108.

[33] E. Ayón-Beato and A. García, Non-singular charged black hole solution for non-linear source, Gen. Relativ. Gravit. **31**, 629 (1999).

[34] E. Ayón-Beato and A. García, New regular black hole solution from nonlinear electrodynamics, Phys. Lett. B **464**, 25 (1999).

[35] E. Ayón-Beato and A. García, The Bardeen model as a nonlinear magnetic monopole, Phys. Lett. B **493**, 149 (2000).

[36] I. Dymnikova, Regular electrically charged vacuum structures with de Sitter centre in nonlinear electrodynamics coupled to general relativity, Classical Quantum Gravity **21**, 4417 (2004).

[37] L. Balart and E. C. Vagenas, Regular black holes with a nonlinear electrodynamics source, Phys. Rev. D **90**, 124045 (2014).

[38] M. E. Rodrigues and M. V. de S. Silva, Bardeen regular black hole with an electric source, J. Cosmol. Astropart. Phys. 06 (2018) 025.

[39] K. A. Bronnikov, Regular magnetic black holes and monopoles from nonlinear electrodynamics, Phys. Rev. D **63**, 044005 (2001).

[40] J. Matyjasek, Extremal limit of the regular charged black holes in nonlinear electrodynamics, Phys. Rev. D **70**, 047504 (2004).

[41] M.-S. Ma, Magnetically charged regular black hole in a model of nonlinear electrodynamics, Ann. Phys. (Amsterdam) **362**, 529 (2015).

[42] Z.-Y. Fan and X. Wang, Construction of regular black holes in general relativity, Phys. Rev. D **94**, 124027 (2016).

[43] S. I. Kruglov, Black hole as a magnetic monopole within exponential nonlinear electrodynamics, Ann. Phys. (Amsterdam) **378**, 59 (2017).

[44] Z.-Y. Fan, Critical phenomena of regular black holes in anti–de Sitter space-time, Eur. Phys. J. C **77**, 266 (2017).

[45] B. Toshmatov, Z. Stuchlík, and B. Ahmedov, Comment on "Construction of regular black holes in general relativity", Phys. Rev. D **94**, 028501 (2018).

[46] G. J. Olmo and D. Rubiera-Garcia, Palatini $f(R)$ black holes in nonlinear electrodynamics, Phys. Rev. D **84**, 124059 (2011).

[47] E. L. B. Junior, M. E. Rodrigues, and M. J. S. Houndjo, Regular black holes in $f(T)$ gravity through a nonlinear electrodynamics source, J. Cosmol. Astropart. Phys. 10 (2015) 060.

[48] M. E. Rodrigues, E. L. B. Junior, G. T. Marques, and V. T. Zanchin, Regular black holes in $f(R)$ gravity coupled to nonlinear electrodynamics, Phys. Rev. D **94**, 024062 (2016); **94**, 049904(A) (2016).

[49] M. V. de S. Silva and M. E. Rodrigues, Regular black holes in $f(G)$ gravity, Eur. Phys. J. C **78**, 18 (2018).

[50] D. P. Sorokin, Introductory notes on non-linear electrodynamics and its applications, Fortschr. Phys. **70**, 2200092 (2022).

[51] K. A. Bronnikov, Regular black holes sourced by nonlinear electrodynamics, arXiv:2211.00743.

[52] M. Mars, M. M. Martń-Prats, and J. M. M. Senovilla, The $2m \leq r$ property of spherically symmetric static spacetimes, Phys. Lett. A **218**, 147 (1996).

[53] O. B. Zaslavskii, Regular black holes and energy conditions, Phys. Lett. B **688**, 278 (2010).

[54] A. Borde, Regular black holes and topology change, Phys. Rev. D **55**, 7615 (1997).

[55] J. Bekenstein, Extraction of energy and charge from a black hole, Phys. Rev. D **7**, 949 (1973).

[56] G. W. Gibbons, Vacuum polarization and the spontaneous loss of charge by black holes, Commun. Math. Phys. **44**, 245 (1975).

[57] T. Nakamura and H. Sato, Absorption of massive scalar field by a charged black hole, Phys. Lett. B **61**, 371 (1976).

[58] C. L. Benone and L. C. B. Crispino, Superradiance in static black hole spacetimes, Phys. Rev. D **93**, 024028 (2016).

[59] Olaf Baake and Oliver Rinne, Superradiance of a charged scalar field coupled to the Einstein-Maxwell equations, Phys. Rev. D **94,** 124016 (2016).

[60] V. Balakumar, E. Winstanley, R. P. Bernar, and L. C. B. Crispino, Quantum superradiance on static black hole space-times, Phys. Lett. B **811,** 135904 (2020).

[61] B. Cuadros-Melgar, R. D. B. Fontana, and J. de Oliveira, Superradiance and instabilities in black holes surrounded by anisotropic fluids, Phys. Rev. D **104,** 104039 (2021).

[62] R. D. B. Fontana, Scalar field instabilities in charged BTZ black holes, arXiv:2306.02504.

[63] R. Brito, V. Cardoso, and P. Pani, Superradiance—the 2020 edition, Lect. Notes Phys. **906,** 1 (2015).

[64] E. Franzin, S. Liberati, J. Mazza, R. Dey, and S. Chakraborty, Scalar perturbations around rotating regular black holes and wormholes: Quasinormal modes, ergoregion instability, and superradiance, Phys. Rev. D **105,** 124051 (2022).

[65] Z. Li, Scalar perturbation around rotating regular black hole: Superradiance instability and quasinormal modes, Phys. Rev. D **107,** 044013 (2023).

[66] W. Unruh, Absorption cross section of small black holes, Phys. Rev. D **14,** 3251 (1976).

[67] J. A. Futterman, F. A. Handler, and R. A. Matzner, *Scattering from Black Holes* (Cambridge University Press, Cambridge, England, 1988).

[68] E. S. Oliveira, L. C. B. Crispino, and A. Higuchi, Equality between gravitational and electromagnetic absorption cross sections of extreme Reissner-Nordström black holes, Phys. Rev. D **84,** 084048 (2011).

[69] C. L. Benone, E. S. de Oliveira, S. R. Dolan, and L. C. B. Crispino, Absorption of a massive scalar field by a charged black hole, Phys. Rev. D **89,** 104053 (2014); **95,** 044035(A) (2017).

[70] L. C. S. Leite, C. L. Benone, and L. C. B. Crispino, Scalar absorption by charged rotating black holes, Phys. Rev. D **96,** 044043 (2017).

[71] L. C. S. Leite, S. R. Dolan, and L. C. B. Crispino, Absorption of electromagnetic and gravitational waves by Kerr black holes, Phys. Lett. **74B,** 130 (2017).

[72] L. C. S. Leite, S. R. Dolan, and L. C. B. Crispino, Absorption of electromagnetic plane waves by rotating black holes, Phys. Rev. D **98,** 024046 (2018).

[73] C. L. Benone and L. C. B. Crispino, Massive and charged scalar field in Kerr-Newman spacetime: Absorption and superradiance, Phys. Rev. D **99,** 044009 (2019).

[74] S. V. M. C. B. Xavier, C. L. Benone, and L. C. B. Crispino, Absorption by stringy black holes, Eur. Phys. J. C **81,** 1127 (2021).

[75] C. F. B. Macedo and L. C. B. Crispino, Absorption of planar massless scalar waves by Bardeen regular black holes, Phys. Rev. D **90,** 064001 (2014).

[76] P. A. Sanchez, N. Bretón, and S. E. P. Bergliaffa, Scattering and absorption of massless scalar waves by Born-Infeld black holes, Ann. Phys. (Amsterdam) **393,** 107 (2017).

[77] S. Fernando, Bardeen–de Sitter black holes, Int. J. Mod. Phys. D **26,** 1750071 (2017).

[78] M. A. A. Paula, L. C. S. Leite, and L. C. B. Crispino, Electrically charged black holes in linear and non-linear electrodynamics: Geodesic analysis and scalar absorption, Phys. Rev. D **102,** 104033 (2020).

[79] H. Salazar, A. García, and J. Plebanski, Duality rotations and type D solutions to Einstein equations with nonlinear electromagnetic sources, J. Math. Phys. (N.Y.) **28,** 2171 (1987).

[80] C. W. Misner, K. S. Thorne, and J. A. Wheeler, *Gravitation* (W. H. Freeman, San Francisco, 1973).

[81] M. A. A. de Paula, L. C. S. Leite, and L. C. B. Crispino, Scattering properties of charged black holes in nonlinear and Maxwell's electrodynamics, Eur. Phys. J. Plus **137,** 785 (2022).

[82] A. García, E. Hackmann, J. Kunz, Claus Lämmerzahl, and A. Macías, Motion of test particles in a regular black hole space-time, J. Math. Phys. (N.Y.) **56,** 032501 (2015).

[83] E. Jung and D. Park, Effect of scalar mass in the absorption and emission spectra of Schwarzschild black hole, Classical Quantum Gravity **21,** 3717 (2004).

[84] R. Wald, *General Relativity* (University of Chicago Press, Chicago, 1984).

[85] B. Toshmatov, A. Abdujabbarov, B. Ahmedov, and Z. Stuchlík, Particle motion and Penrose processes around rotating regular black hole, Astrophys. Space Sci. **357,** 41 (2015).

[86] S. R. Dolan, M. A. A. de Paula, L. Leite, and L. C. B. Crispino, Superradiant instability of a charged regular black hole, arXiv:2401.14967.

[87] K. Akiyama *et al.* (Event Horizon Telescope Collaboration), First Sagittarius A* Event Horizon Telescope results. I. The shadow of the supermassive black hole in the center of the Milky Way, Atrophys. J. **930,** L12 (2022).

[88] H.-P. Gu, H.-T. Wang, and L. Shao, Constraints on charged black holes from merger-ringdown signals in GWTC-3 and prospects for the Einstein Telescope, Phys. Rev. D **109,** 024058 (2024).

[89] J. Barranco, A. Bernal, J. C. Degollado, A. D.-T., M. Megevand, M. Alcubierre, D. Núñez, and O. Sarbach, Are black holes a serious threat to scalar field dark matter models?, Phys. Rev. D **84,** 083008 (2011).

[90] J.-T. Li and T. Lin, Dynamics of millicharged dark matter in supernova remnants, Phys. Rev. D **101,** 103034 (2020).